Observations Regarding the Synthesis and Redox Chemistry of Heterobimetallic Uranyl Complexes Containing Group 10 Metals

*Emily R. Mikeska, Natalie M. Lind, Alexander C. Ervin, Celine Khalife, Joseph P. Karnes, and James D. Blakemore**

Department of Chemistry, University of Kansas, 1567 Irving Hill Road, Lawrence, Kansas 66045, United States

* To whom correspondence should be addressed: blakemore@ku.edu (J.D.B.)

KEYWORDS: crystallography • electrochemistry • protonolysis • uranium • nickel

Abstract

Literature reports have demonstrated that Schiff-base-type ligands can serve as robust platforms for the synthesis of heterobimetallic complexes containing transition metals and the uranyl dication (UO_2^{2+}). However, efforts have not advanced to include either synthesis of complexes containing second- or third-row transition metals or measurement of the redox properties of the corresponding heterobimetallic complexes, despite the significance of actinide redox in studies of nuclear fuel reprocessing and separations. Here, metalloligands denoted **[Ni]**, **[Pd]**, and **[Pt]** that contain the corresponding Group 10 metals have been prepared and a synthetic strategy to access species incorporating the uranyl ion (UO_2^{2+}) has been explored, toward the goal of understanding how the secondary metals could tune uranium-centered redox chemistry. The synthesis and redox characterization of the bimetallic complex **[Ni,UO_2]** was achieved, and factors that appear to govern extension of the chosen synthetic strategy to complexes with Pd and Pt are reported here. Infrared and solid-state structural data from X-ray diffraction analysis of the metalloligands **[Pd]** and **[Pt]** show that the metal centers in these complexes adopt the expected square planar geometries, while the structure of the bimetallic **[Ni,UO_2]** reveals that the uranyl moiety influences the coordination environment of Ni(II), including inducement of a puckering of the ligand backbone of the complex in which the phenyl rings fold around the nickel-containing core in an umbrella-shaped fashion. Cyclic voltammetric data collected on the heterobimetallic complexes of both Ni(II) and Pd(II) provide evidence for uranium-centered redox cycling, as well as for the accessibility of other reductions that could be associated with Ni(II) or the organic ligand backbone. Taken together, these results highlight the unique redox behaviors that can be observed in multimetallic systems and design concepts that could be useful for accessing tunable multimetallic complexes containing the uranyl dication.

Introduction

Control over actinide redox chemistry is crucial in the tuning of solubility, reactivity, and speciation of actinide-containing complexes in solution.[1] Useful separations have been achieved through redox-induced changes in speciation, and thus understanding how actinide redox chemistry can be tuned could offer a promising route to improved nuclear fuel reprocessing strategies.[2] As the redox chemistry of actinides also governs their speciation in the environment, there appear to be many opportunities where ligand design and optimization of conditions where actinides are present could be used toward new strategies for environmental remediation. For uranium in particular, the prevalent species under most conditions is the uranyl dication (UO_2^{2+}), prompting much work focused on influencing the properties of this species.[3] Uranyl has proven to be a challenging target, however, as the *trans*-dioxo ligands impart great stability to the +6 oxidation state and are difficult to functionalize or remove.[4] No doubt motivated by these applications and challenges, there have been many reports on strategies aimed at enabling reduction of uranium(VI) including innovations in ligand design,[5] oxo activation,[6] and functionalization.[7]

While several reports of redox in monometallic systems exist,[8] the understanding of uranium-based redox in bimetallic systems is much more limited.[9] Our group has previously reported tuning the reduction potential of the $U^{VI/V}$ couple by the installation of Lewis acidic, redox-inactive cations in close proximity to the uranyl ion.[10] The influence exerted by the secondary redox-inactive cations could be quantified through the descriptor of these ions' Lewis acidities, as judged by the pK_a values of the corresponding metal aqua cations. The supporting ligand in the noted study was macrocyclic in nature, and incorporation of the secondary ions resulted in a systematic shift of –61 mV/pK_a in the U(VI)/U(V) reduction potential. This influence can be understood to

arise from a charge density effect wherein the secondary cations modulate the donor power of bridging phenoxide ligands that are a key feature of the ligand core.[11] Complementing this work, a few structural reports are available on the assembly of bimetallic complexes of uranyl with redox-active transition metals held in close proximity. Perhaps the most important examples are those described by Vigato and Ephritikhine in the 1990s and early 2000s.[12,13] In these complexes, a transition metal was housed in a tetradentate [N_2O_2] Schiff base cavity with an adjacent tetradentate [O_2O_2] cavity composed of two formally *L*-type phenoxides and two *X*-type phenoxides poised for binding uranyl. In this instance, these compounds were studied for their magnetic properties, but their electrochemical properties were not interrogated. To the best of our knowledge, there is only one report of the electrochemical properties of heterobimetallic complex containing uranyl and another redox-active metal; the noted complex features U(VI) paired with iron(II).[14] Furthermore, we are aware of no studies in which uranium(VI) is paired with a second or third row transition metals in a molecular complex.

With all of these observations in mind, our attention was drawn to appealing and robust synthetic chemistry developed by Ephritikhine to access a nickel-uranyl bimetallic complex, denoted **[Ni,UO_2]•H_2O**, that was structurally characterized.[13] However, the synthetic route to access the complex relies on a water- and air-sensitive U(IV) starting material to generate the uranyl dication that is ultimately incorporated into the product; oxidation appears to have been achieved in the literature work by adventitious H_2O and/or O_2 present under the synthetic conditions. In light of these observations, we envisioned that a more direct route to heterobimetallic compounds of the Vigato-Ephritikhine type could be achieved through use of an appropriate U(VI) reagent; we imagined that such a procedure could be extended to metalloligands based on the other Group 10 metals (Pd, Pt) as well, affording the opportunity to compare trends

among these related metals. We anticipated that an interrogation of the electrochemical properties of complexes targeted in this effort could also shed light on the accessible redox chemistry of uranium when held in multimetallic systems, an area that has received less attention than it deserves.

Here, we report the synthesis and characterization of a series of Group 10 metal-containing metalloligands and their propensity toward incorporation of the uranyl dication, UO_2^{2+}. Preparation and characterization of salen-type metalloligand precursors **[Ni]**, **[Pd]**, and **[Pt]** confirmed the coordination of each Group 10 metal in the tetradentate [N_2,O_2] Schiff base site of the organic framework that is characteristic of salen ligands. Investigations into their reactivity with uranyl acetate dihydrate ($UO_2(OAc)_2$•$2H_2O$) show that complexes of nickel(II) and palladium(II) with uranyl are isolable under the chosen conditions. Additionally, data suggest that an adduct of platinum(II) and UO_2^{2+} may form when uranyl triflate is used as the uranium-containing precursor,[15] as observed by ^{1}H NMR spectra in CD_3CN; the apparent adduct decomposes, however, upon exposure to tetrahydrofuran. Solid-state infrared spectra of **[Ni,UO_2]** and **[Pd,UO_2]** demonstrate that uranyl is in a similar environment in both instances, X-ray diffraction data collected for **[Ni,UO_2]** show the formation of a dimeric form of the complex in the solid state, complementing Ephritikhine's prior report[13] on the structure of a monomeric form of the complex. The electrochemical properties of the metalloligand precursors and the related uranyl bimetallic complexes were also studied, revealing two accessible redox manifolds in both **[Ni,UO_2]** and **[Pd,UO_2]**. Observations suggest that one of the accessible redox processes could be attributable to uranium-centered reduction. Taken together, these observations suggest that bimetallic systems are useful for the study of uranium redox chemistry and underscore the utility of protonolysis reactivity for accessing such structures.

Results

Synthesis and characterization of metalloligands and bimetallic uranyl complexes. While transition metal complexes of salen-type ligands are well known,[16,17] we envisioned generating a homologous series of Group 10 transition metal (Ni, Pd, Pt) complexes with secondary binding cavities to enable a systematic study of the reactivity of these bimetallic complexes with uranyl (see Scheme 1). As demonstrated in a prior report by Vigato & co-workers, **[Ni]** forms readily in a one-pot reaction of the ligand components and $Ni(OAc)_2$; in our hands, this procedure yield a product whose ^{1}H NMR spectrum was consistent with the binding of nickel(II) into the desired tetradentate [N_2,O_2] cavity and prior characterization available for this compound (see SI, Figure S3).[12] Conversely, the analogous complex **[Pd]** must be generated from the reaction of the isolated ligand $\mathbf{L^{OH}}$ and $[Pd(OAc)_2]_3$ as previously demonstrated by our group for a related macrocyclic ligand system.[18] This reaction proceeds in high yield and the NMR spectra of the isolated material, as well as corresponding elemental analysis data, are consistent with formation of this complex and the successful incorporation of palladium(II) (see SI, Figure S10–S15). Attempts to extend the synthesis to platinum, however, using $\mathbf{L^{OH}}$, potassium tetrachloroplatinate (K_2PtCl_4), and an exogenous base, sodium acetate, resulted in ligand decomposition based on the apparent generation of Pt nanoparticles in the reaction vessel; ligand decomposition products were also observed via ^{1}H NMR. The generation of Pt nanoparticles under these conditions was implied by our observation of very dark heterogeneous material in reaction flasks; indeed, K_2PtCl_4 is often used explicitly for Pt nanoparticle generation in the presence of ascorbic acid and other similar reducing reagents.[19,20] Furthermore, Pt nanoparticles are known to catalyze the oxidation of phenols and many reports of the oxidation of salen-type ligands exist.[21,22] In light of all these

findings, we opted to prepare a related platinum complex denoted **[Pt]**, which can be synthesized from metalation of a related ligand, $\mathbf{L^{OMe}}$. Substituting *o*-vanillin for 2,3-dihydroxybenzaldehyde and metalating with bis(dimethylsulfoxide)platinum(II) chloride ($PtCl_2DMSO_2$) enabled the isolation of the complex, with ^{1}H NMR data and elemental analysis confirming its expected formulation (See SI, Figure S17–S22).

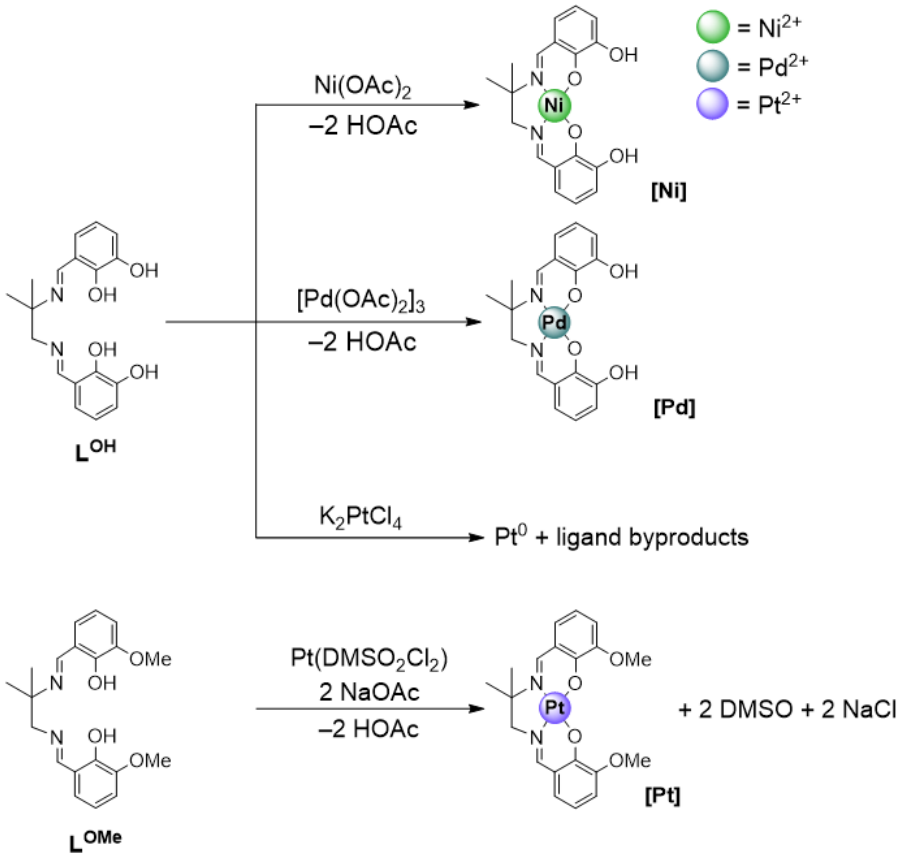

Scheme 1. Synthetic route to access metalloligand precursors **[Ni]**, **[Pd]**, and **[Pt]**.

With the set of three metalloligands in hand, we investigated their reactivity with uranyl. Our group has previously relied on uranyl acetate as a metalating reagent in the preparation of uranyl complexes, taking advantage of its intrinsic disposition toward protonolysis reactivity; we hypothesized that this strategy could be useful for the synthesis of the bimetallic complexes targeted in this study (Scheme 2).[10,23] Indeed, refluxing the metalloligand **[Ni]** with

$UO_2(OAc)_2$•$2H_2O$ in acetonitrile (MeCN) yielded the desired **[Ni,UO_2]** complex in moderate yield. Both ^{1}H NMR and elemental analysis of the product are consistent with the incorporation of uranyl into the dianionic [*O2,O2*] cavity provided by the doubly deprotonated metalloligand, along with the binding of an additional solvent molecule to fulfill equatorial penta-coordination environment of U(VI) (see the Experimental Section and the SI, Figure S4). When the same reaction conditions were applied to **[Pd]** with $UO_2(OAc)_2$•$2H_2O$, **[Pd,UO_2]** appeared to be formed but the desired product was generated along with a persistent 15% impurity of the starting **[Pd]**. Screening of various reaction conditions did not lead to significant improvements in any case (varied stoichiometries of **[Pd]** and uranyl acetate dihydrate; varied reaction temperatures from room temperature to refluxing conditions; varied times from 4 hours to 3 days; use of various solvents, including acetonitrile, N,N-dimethylformamide, dimethylsulfoxide, and water. Additionally, screening of various purification procedures (precipitation from a cooled reaction, precipitation from a concentrated solution by non-polar solvents, washing with polar solvents, and bulk recrystallization) did not yield pure samples of **[Pd,UO_2]** (see SI, Figure S16).[24] We also note here that the bimetallic compounds generated upon metalation of **[Ni]** and **[Pd]** with uranyl display very limited solubility in most organic solvents, restricting the choice of solvents for solution phase characterization to DMF and DMSO for **[Ni,UO_2]** and only DMSO for **[Pd,UO_2]**.

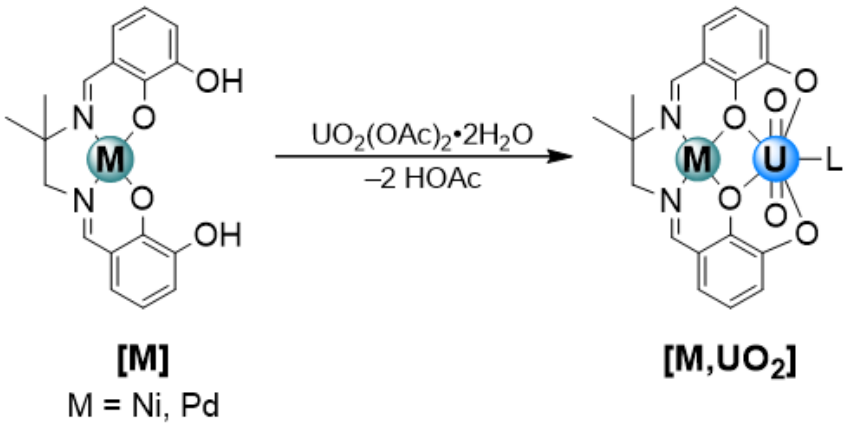

Scheme 2. Synthetic route to accessing **[Ni,UO$_2$]** and **[Pd,UO$_2$]** heterobimetallic complexes employing protonolysis reactivity with $UO_2(OAc)_2$•$2H_2O$.

With low solubility that impeded facile characterizations in the solution phase, we pivoted our focus to solid-state infrared spectroscopy to learn more about the isolated products of our study. Spectra in KBr media were collected to probe perturbations in the reliable asymmetric uranyl stretch or in the ligand vibrational frequencies induced by the presence of the transition metal centers or uranyl (see SI, Figures S24–S31). Metalation of $\mathbf{L^{OH}}$ with nickel(II) and palladium(II) did not give rise to any measurable change in the C=N_{imine} stretching frequency compared to that found in free $\mathbf{L^{OH}}$, but a shift of 14 cm^{-1} in the case of **[Ni,UO$_2$]** and 11 cm^{-1} in the case of **[Pd,UO$_2$]** could be observed upon metalation with uranyl (see SI, Table S1). This behavior is consistent with the dicationic nature of uranyl in that it could exert an effect on the ligand backbone via direction interaction with the phenoxide moieties derived from 2,3-dihydroxybenzaldehyde, thereby shifting the noted vibrational frequencies to a lower energy. A shift in the asymmetric stretch of the UO_2^{2+} unit for **[Ni,UO$_2$]** and **[Pd,UO$_2$]** is shown in Figure 1, which compares spectra for the complexes to that of the starting material $UO_2(OAc)_2$•$2H_2O$; the measured changes are consistent with the incorporation of uranyl into the metalloligands in that the apparent strength of the U–O bond is decreased slightly upon coordination to the metalloligand ($\Delta\tilde{\nu}$ = 29 cm^{-1}, 3.6

meV). Notably, the frequencies of the asymmetric stretches of the UO_2^{2+} units in the spectra of **[Ni, UO_2]** and **[Pd, UO_2]** are identical, an observation which is in accord with the similar coordination environment of uranyl in both complexes.

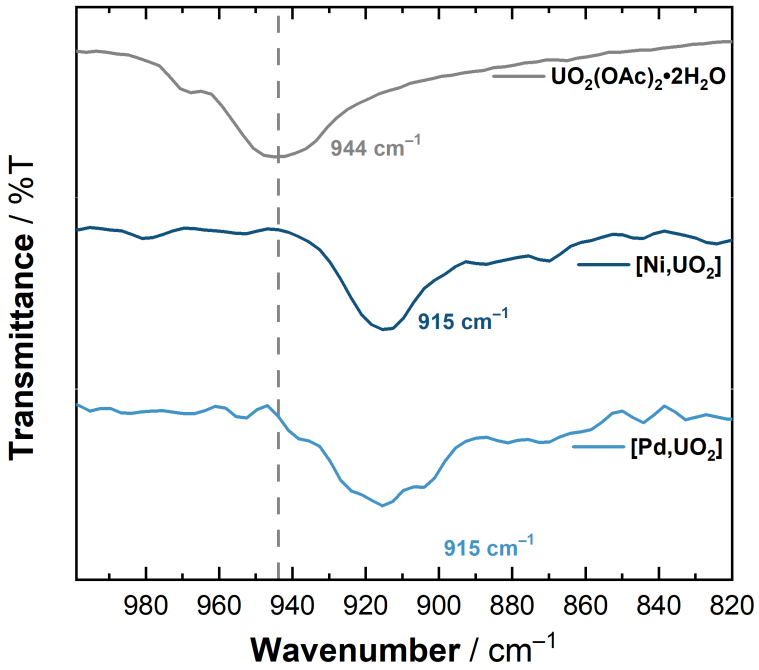

Figure 1. Solid IR spectra of $UO_2(OAc)_2$•$2H_2O$ (top), **[Ni,UO_2]** (middle), and **[Pd,UO_2]** (bottom) in KBr confirming the incorporation of UO_2^{2+} into **[Ni]** and **[Pd]**.

*Solid State structures of **[Pd]**, **[Pt]**, and **[Ni,UO_2]**.* X-ray diffraction (XRD) analysis of **[Pd]** and **[Pt]** confirmed the desired square-planar coordination environment of the transition metal in both cases as shown in Figure 2. Single crystals suitable for XRD analysis of **[Pd]** were grown by vapor diffusion of pentane into a solution of **[Pd]** in tetrahydrofuran while vapor diffusion of diethyl ether into an acetonitrile solution of **[Pt]** afforded suitable crystals of this complex for analysis. Structural details on these complexes are shown in Table 1 and details regarding the crystallography are given in the Supporting Information (pp. S30–S35 and Table S3).

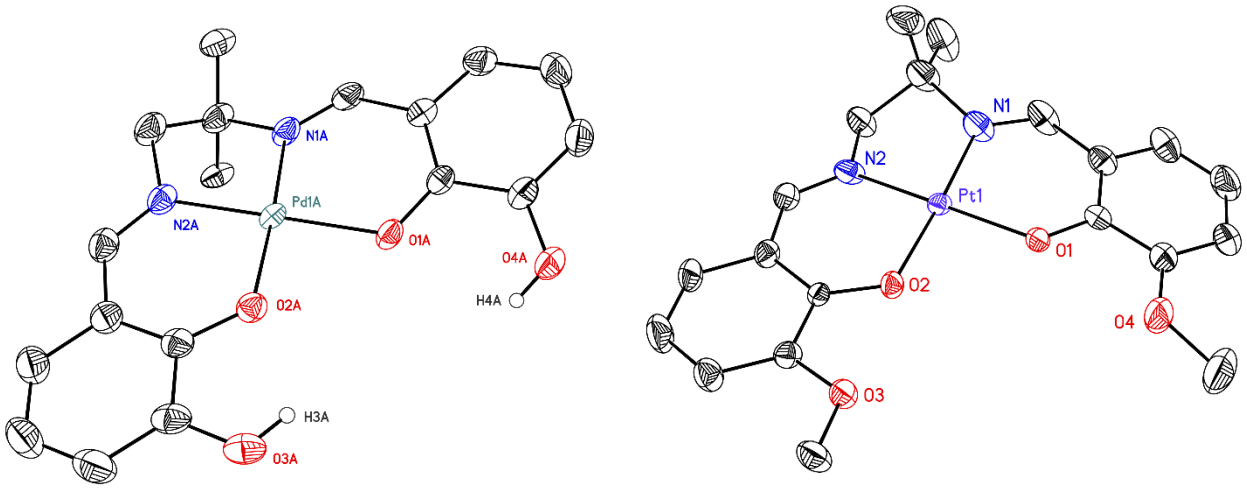

Figure 2. Solid-state structures (XRD) of **[Pd]** and **[Pt]**. For **[Pd]**, all hydrogen atoms except H3A and H4A, a co-crystallized tetrahydrofuran molecule, and a second molecule of the palladium complex found in the asymmetric unit are omitted for clarity. For **[Pt]**, all hydrogen atoms are omitted for clarity. Displacement ellipsoids are shown at the 50% probability level.

Table 1. Comparison of selected structural parameters from X-ray diffraction analysis of **[Ni]**, **[Pd]**, **[Pt]**, **[Ni,UO_2]**, and **[Ni,UO_2] • H_2O**.

	[Ni]	**[Pd]**	**[Pt]**	**[Ni,UO_2]**	**[Ni,UO_2] • H_2O**
Reference	*Reference 12*	*This Work*	*This Work*	*This Work*	*Reference 13*
Z′	1	2	1	2	1
M–N1$_{average}$ (Å) [a]	1.857(4)	1.959(3)	1.949(8)	1.838(4)	1.807(9)
M–N2$_{average}$ (Å) [a]	1.845(4)	1.954(2)	1.952(8)	1.838(5)	1.861(10)
M–O1$_{average}$ (Å) [a]	1.857(3)	2.002(2)	2.001(6)	1.828(4)	1.829(7)
M–O2$_{average}$ (Å) [a]	1.856(3)	1.990(2)	2.003(6)	1.848(3)	1.831(6)
O1•••O2 (Å) [a]	2.513(5)	2.761(3)	2.774(8)	2.376(5)	2.337(9)
U–O5$_{oxo}$ (Å) [a]	–	–	–	1.774(4)	1.790(6)
U–O6$_{oxo}$ (Å) [a]	–	–	–	1.782(4)	1.786(6)
U–O3$_{Ligand}$ (Å) [a]	–	–	–	2.357(3)	2.368(5)
τ_4	0.016	0.039	0.014	0.039	0.035
χ (°) [a, b]	4.8(2)	7.05(6)	8.6(4)	12.4(2)	1.6(3)

[a] Value in parentheses refers to the e.s.d. that is the largest for an individual entry among the independent values used to compute the average.
[b] Defined as the fold angle (see reference 17) between the centroids of the phenyl rings in each structure. Specifically, it is the angle between the centroid of the mean plane defined by C2, C3, C4, C5, C6, and C7 and the mean plane defined by C8, C9, C10, C11, C12, and C13 with the center point of the angle being a point on a plane normal to and centered on a line connecting the centroids of the two previously defined planes.

In the structures of **[Pd]** and **[Pt]** reported here as well as in the structure of **[Ni]** reported by Ephritikhine, the M(II) ions (M = Ni, Pd, and Pt) remain in strictly square planar environments with values of the τ_4 geometry index for these compounds very close to ideal for the square planar geometry (Table 1).[12,25] Although situated in virtually identical coordination environments, the M–N and M–O distances in **[Pd]** and **[Pt]** are longer than those of **[Ni]**, which is anticipated on the basis of their larger radii as second and third row transition metals (ionic radii of square planar, four-coordinate ions: Ni^{2+} = 49 pm; Pd^{2+} = 64 pm; Pt^{2+} = 60 pm).[26] This size difference also results in a widening of the O1•••O2 gap (an increase of 0.25 Å in the case of **[Pd]** and 0.26 Å in the case of **[Pt]** compared to **[Ni]**) and a slight puckering in the overall structures as quantified by the fold angle (χ) between the mean planes of the two phenyl rings found in each structure (Table 1). Although quantified in a variety of ways, this umbrella-like puckering is commonly encountered in complexes of Schiff-base salen ligands with transition metals.[17]

The structure of **[Pd]** also features a rich hydrogen bonding network built on the availability of the phenol moieties (associated with O3A/B and O4A/B). The phenols engage in H-bonding in a pairwise fashion; there are two molecules of **[Pd]** present in the asymmetric unit and they appear to be held together through H-bonding (see Figure 3). (There are no water molecules found in the structural data for this complex.) Weak electrostatic interactions which appear to influence the long-range packing of the crystal can also be measured between a disordered outer-sphere tetrahydrofuran (THF) and the main **[Pd]** moieties of the asymmetric unit. One orientation of the THF molecule interacts with the imine proton and a phenyl proton (O1S•••C1B: 3.377(6) Å and O1S•••C3B: 3.466(4) Å), while the other orientation interacts with the imine proton and a methyl proton (O1S'•••C1B: 3.316(14) Å and O1S'•••C18B: 3.294(18) Å; see SI, Figure S54).[27] And, although **[Pt]** does not feature any free phenolic protons, weak electrostatic interactions could be

measured between **[Pt]** molecules on the basis of moderate donor-acceptor distances; these interactions likely influence long-range packing (O1A•••C12B: 3.433(11) Å, O2A•••C14B: 3.015(10) Å, O3A•••C15B: 3.414(10) Å; see SI, Figure S56).[28]

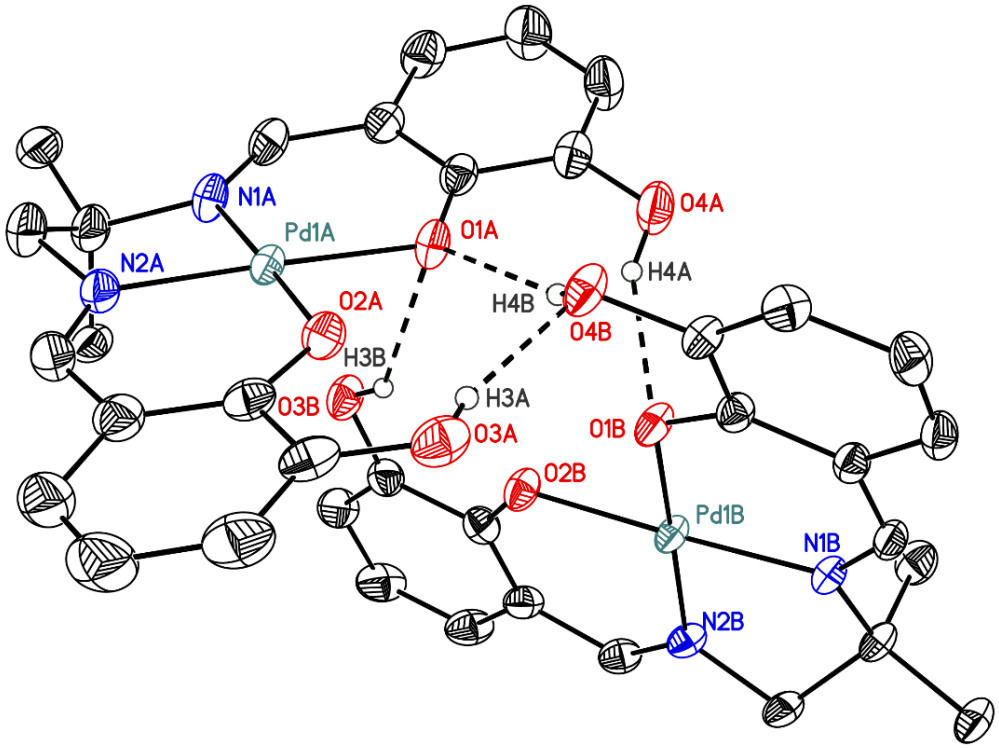

Figure 3. Solid-state structure (XRD) of **[Pd]**. Hydrogen bonding interactions between adjacent **[Pd]** molecules are shown with dashed lines. All hydrogen atoms not engaged in hydrogen bonding as well as a disordered outer-sphere co-crystallized tetrahydrofuran molecule are omitted for clarity. Displacement ellipsoids are shown at the 50% probability level.

Single crystals suitable for X-ray diffraction analysis were obtained for **[Ni,UO$_2$]** from vapor diffusion of diethyl ether into a concentrated solution of the complex in dimethylformamide. Structural details for this structure can be found in Table 1 and details on the crystallography are given in the Supporting Information (pp. S36–S37 and Table S3). Although the nickel(II) center

experiences little distortion of its coordination environment upon incorporation of UO_2^{2+} into the adjacent site on the basis of the similar values of the τ_4 geometry index of **[Ni]** and **[Ni,UO$_2$]**, contractions in both the M–N1 and M–O1 bond lengths indicate that the Ni(II) ion is positioned asymmetrically within its tetradentate cavity in **[Ni,UO$_2$]** compared to **[Ni]** (Δ_{Ni-N1} = 0.02 Å; Δ_{Ni-O1} = 0.028 Å). In accord with the binding of uranyl into the open site of **[Ni]** and the drawing together of the heterobimetallic diamond core motif, a contraction in the O1•••O2 distance was measured ($\Delta_{O1\cdots O2}$ = 0.137 Å); this contraction appears to drive further puckering of the ligand backbone in **[Ni,UO$_2$]**, leading to an increase in χ from 4.8(2)º in **[Ni]** to 12.4(2)º in **[Ni,UO$_2$]**. Consistent with the robust nature of UO_2^{2+} established in much prior work, the uranyl unit remains intact upon coordination to **[Ni]**, as evidenced by U–O_{oxo} bond lengths of 1.774(4) and 1.782(4) Å; these distances are in agreement with well-documented, typical bond metrics for other U(VI) complexes.[29]

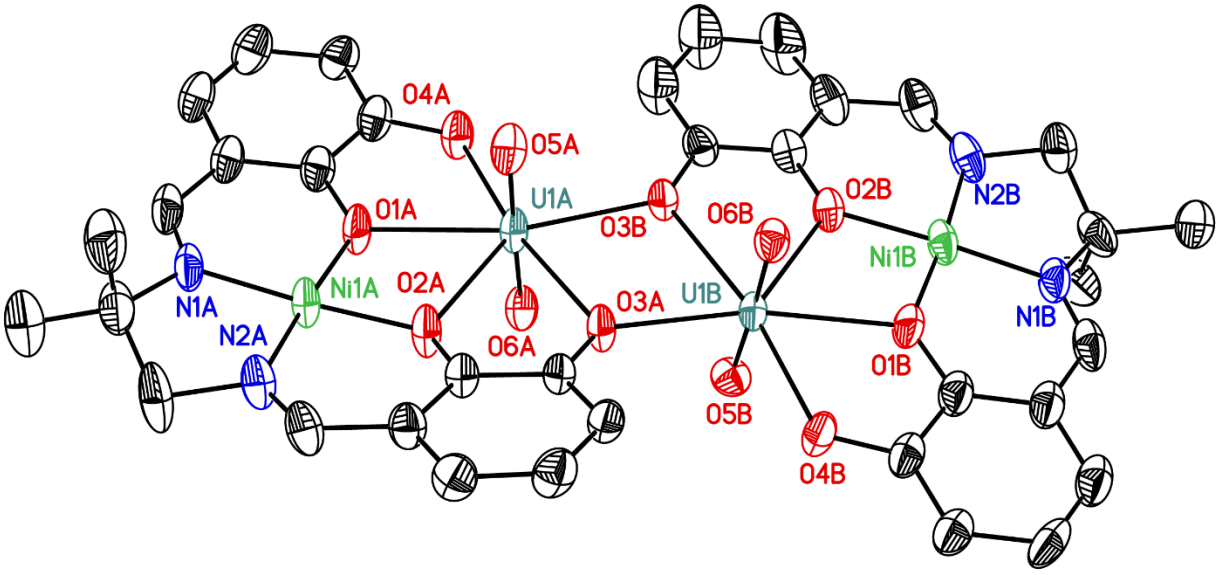

Figure 4. Solid-state structure (XRD) of **[Ni,UO$_2$]**. All hydrogen atoms and two co-crystallized outer-sphere dimethylformamide molecules found in the asymmetric unit are omitted for clarity. Displacement ellipsoids are shown at the 50% probability level.

While the structural parameters describing the Ni(II) and U(VI) sites in **[Ni,UO$_2$]** are similar to those found in the reported structure of **[Ni,UO$_2$]•H$_2$O** from Ephritikhine,[13] a major difference can be observed in the packing of the structures. As shown in Figure 4, the asymmetric unit of **[Ni,UO$_2$]** is a dimeric species which features a phenoxide joined to a nearby U, fulfilling the equatorial coordination needs of U(VI), while the asymmetric unit of **[Ni,UO$_2$]•H$_2$O** is monomeric with a water molecule as the fifth ligand in the equatorial belt of U (see SI, Figure S50).[13] Consistent with differences in the charge density between a water and a partially charged phenoxide moiety, the U–O3$_{Ligand}$ distance is shorter in the case of **[Ni,UO$_2$]** (Table 1). An additional contribution to the difference in U–O3$_{Ligand}$ distances comes from the apparent engagement of the bound water molecule of **[Ni,UO$_2$]•H$_2$O** in hydrogen bonding interactions with the adjacent (symmetry-generated) molecule and with outer-sphere pyridine molecules present in Ephritikhine's structure of **[Ni,UO$_2$]•H$_2$O** (see SI, Figure S50).

In the case of **[Ni,UO$_2$]** reported here, the long-range packing is strongly influenced by a series of intrinsically weak hydrogen bonding interactions that could be measured between the oxo's of the two uranyl units found in the crystallized form of the complex and protons of the adjacent molecules. These interactions do not appear to markedly impact the U–O$_{oxo}$ bond strength as the U–O$_{oxo}$ bond distances remain reliably within the reported range for U(VI)–O$_{oxo}$ bond lengths (*vide supra*).[27,28] These weak hydrogen bonding interactions feature a central **[Ni,UO$_2$]** unit that engages with its six surrounding symmetry-generated neighbors, acting as both an acceptor through the oxo's of the uranyl unit and a donor through its imine, aromatic, and methylene protons (see SI, Figure S59–S64). As the protons in these structures were generated with fixed positions using idealized riding models pinned to their respective non-hydrogen atoms, the interactions discussed here have been quantified in terms of the donor–acceptor distances; these range from 3.150(7) Å

for the interactions with the imine protons to 3.528(8) Å for the interactions with the aromatic protons, with an intermediate value of 3.358(7) Å for the interactions with the methylene protons (average value of all interactions measured is reported here with individual values reported in the SI, Table S2). Taken together, the available structural data highlight the robust nature of the ligands used in this work, their unique ability to support bimetallic systems, and the role that hydrogen bonding can play in the packing and long-range order of these structures.

Electrochemistry. After obtaining the structural data described above, we moved to interrogate the electrochemical properties of the metalloligands and **[Ni,UO$_2$]**. Cyclic voltammetry data for **[Ni]** in DMF-based electrolyte reveal a single accessible redox event at $E_{1/2}$ = –1.99 V (all potentials quoted vs. ferrocenium/ferrocene; denoted hereafter as $Fc^{+/0}$), consistent with a nickel-centered reduction (Figure 5).[30] This couple appears to be chemically reversible and electrochemically quasi-reversible on the basis of the small peak-to-peak separation measured (ΔE_p = 80 mV); scan rate-dependent data suggest that both the oxidized and reduced forms of the complex are freely diffusional in solution (see SI, Figure S37). Conversely, cyclic voltametric data for **[Pd]** show an irreversible reductive feature at $E_{p,c}$ = –2.3 V, which is consistent with ligand centered reduction of **[Pd]** based on the known propensity for palladium complexes of this type to undergo ligand centered reduction at similar potentials and the similarity of the data to that of $\mathbf{L^{OH}}$ ($E_{p,c}$ = –2.1 V; see SI, Figures S32 & S38).[18] Minor currents associated with the re-oxidation of the reduced form of **[Pd]** could be observed around –2.2 V at faster scan rates, consistent with an irreversible reduction in which a chemical process whose kinetics on the order of the timescale of the cyclic voltammetry experiment follows the electrochemical reduction (see SI, Figure S39). In a similar fashion, cyclic voltametric data for **[Pt]** display an irreversible cathodic feature at $E_{p,c}$ = –2.3 V consistent with a ligand-centered reduction (see SI, Figures S40 & S41).

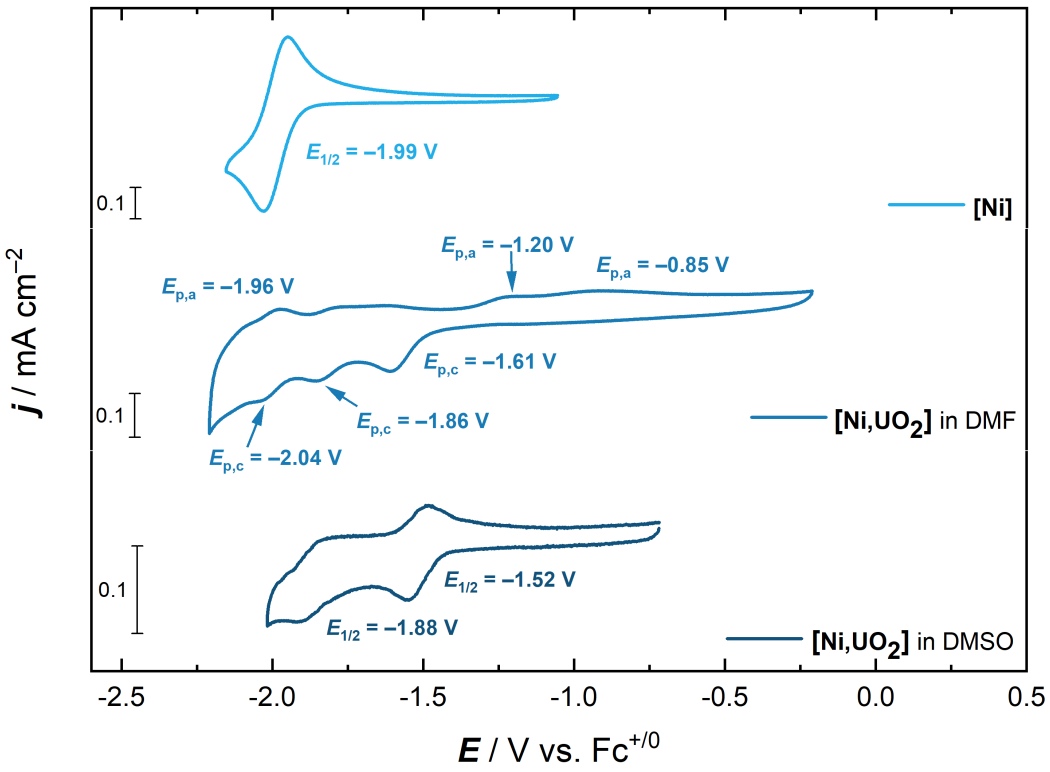

Figure 5. Cyclic voltammetry data for **[Ni]** in DMF electrolyte (top), **[Ni,UO$_2$]** in DMF electrolyte (middle), and **[Ni,UO$_2$]** in DMSO electrolyte (bottom). Electrolyte: 0.1 M $[^nBu_4N]^+[PF_6]^-$; scan rate: 100 mV/s.

Several accessible reduction events are observable in the cyclic voltametric data collected for **[Ni,UO$_2$]** in DMF-based electrolyte. These events include reduction waves that peak at potentials of –1.61 V and –1.86 V and corresponding re-oxidation peak potentials at –0.85 V and –1.20 V, respectively (Figure 5). The presence of two cathodic features suggest that both nickel and uranium undergo could reduction in this system, a hypothesis that is consistent with previously reported potential ranges for reduction events for both nickel and uranyl in similar ligand frameworks.[10,18,23,31,3210] Scanning further negative toward the cathodic limit of the conditions used here revealed an additional redox event at $E_{1/2}$ = –2.0 V, whose reversible nature and virtually identical potential matches the electrochemical behavior of **[Ni]**, suggesting the possibility that

there is some degree of dissociation of the uranyl ion from **[Ni,UO$_2$]** upon reduction of U(VI) to generate U(V). Altering the conditions to DMSO-based electrolyte, however, reveals a much simpler voltammogram as seen in Figure 5, indicating that the accessible reduced form(s) of **[Ni,UO$_2$]** may be stabilized by DMSO. Indeed, scan rate-dependent data for **[Ni,UO$_2$]** in DMSO-based electrolyte demonstrate diffusional behavior for the reduced and oxidized forms of the complexes associated with both redox couples present in the data (see SI, Figure S44). The first redox couple observed in DMSO-based electrolyte appears highly reversible on the basis of the near ideal peak-to-peak separation (70 mV) and is likely associated with reduction of U(VI) to U(V) given its similar reduction potential to that of other similar uranyl complexes (see SI, Figure S44).[23,31,32] However, some chemical reactivity occurs upon the second reduction as evidenced by the lack of current associated with re-oxidation except at faster scan rates (see SI, Figure S45).

Cyclic voltametric data for **[Pd,UO$_2$]** could not be obtained in DMF-based electrolyte because of the low solubility of the complex in this solvent. However, modest solubility of the complex in DMSO enabled exploration of its redox chemistry in electrolyte based on that solvent. Similar to the case of **[Ni,UO$_2$]**, the cyclic voltammogram of **[Pd,UO$_2$]** (used for the experiment in the form of its admixture with co-isolated **[Pd]**, *vide supra*) revealed two reductive features at –1.52 V and –1.86 V with corresponding re-oxidations at –1.44 V and –1.78 V, respectively (see SI, Figure S46–S48). While the observation of two features suggests that both uranium and the ligand backbond could feature accessible reductions in this window, it is evident that chemical reactivity takes place upon reduction following multiple excursions to negative potentials (see SI, Figure S49). Scanning to cathodic potentials over the course of at least 10 minutes gives rise to decreases in the currents associated with both features, a likely indicator that the UO_2^+ dissociates following the second reduction, despite the stabilizing characteristics of DMSO in the related **[Ni,UO$_2$]**

compound. Nevertheless, these data are consistent with the an initial U-centered reduction followed by a ligand-based reduction given the known propensity for complexes of this type containing Pd(II) to undergo reduction at the ligand (leading to chemical reactivity) prior to reduction of Pd(II).[18] In any case, we wish to be clear that we are reporting these data obtained with the admixture of **[Pd,UO$_2$]** and **[Pd]** here primarily for comparison to the data obtained on pure **[Ni,UO$_2$]**.

Discussion

Previous reports from the groups of Ephritkhine and Vigato established the ability to access heterobimetallic complexes of transition metals with uranyl, but no electrochemical data for these complexes have been available. We are also unaware of prior extensions of such investigations into studies including second- or third-row transition metals. With the accessibility of bimetallic complexes known for first-row transition metals, we set out here to pursue evidence regarding how to extend studies to include later transition metals. We also hoped to pursue electrochemical studies of unique systems containing multiple redox-active moieties. In the part of our work in this area reported here, we have been able to prepare three metalloligands/precursors and access a bimetallic nickel–uranyl complex, **[Ni,UO$_2$]**, by a facile synthetic route. We observed a unique asymmetric unit and crystal packing for the compound in the solid-state structure; comparison of our data to those from a prior structure of thecomplex obtained by Ephritikhine highlights the diverse modes of interactions accessible to uranyl compounds of this general type, including the tendancy for ligands to bridge between the highly Lewi acidic U(VI) centers in the complexes.[33]

While electrochemical studies of the metalloligands displayed the anticipated metal- and ligand-centered reductions in the cases of **[Ni]** and **[Pd]**/**[Pt]**, respectively, data for the bimetallic complexes of **[Ni,UO$_2$]** and **[Pd,UO$_2$]** demonstrated the greater level of complexity that can be

encountered in electrochemical properties of multimetallic systems. Preliminary cathodic sweeps in DMF-based electrolyte revealed significant instability of the reduced form(s) of **[Ni,UO_2]**, indicative of uranyl dissociation upon reduction based on the observation of **[Ni]** in the solution at more negative potentials. On the other hand, cyclic voltammetry of **[Ni,UO_2]** in electrolyte based on DMSO led to the observation of two distinct couples which both displayed greater reversibility and stability; this improved behavior could result from the anticipated highly coordinating nature of DMSO, although further study is needed to identify the precise origins of the solvent-dependent electrochemical behavior. In voltammetry of both **[Ni,UO_2]** and **[Pd,UO_2]** in DMSO electrolyte, two reductive features with corresponding oxidations were measured, highlighting the ability to access both uranyl- and Ni(II)-centered reductions in the case of **[Ni,UO_2]** and possible uranyl- and ligand-centered reductions in the case of **[Pd,UO_2]**. Further explorations into the electrochemical and chemical processes that can be induced in heterobimetallic systems containing transition metals and the uranyl dication appear to be attractive for further study.

Finally, while **[Ni,UO_2]** displays modest solubility that enabled characterization in both solutions and in the solid state, attempts to incorporate uranyl into **[Pd]** ultimately yielded materials that were highly insoluble and difficult to purify. The family of salen-type ligands featuring an [O_2O_2] cavity of two formally *L*-type phenoxides and two *X*-type phenoxides seemed attractive for the targeted synthesis of bimetallic uranyl complexes at first, but these species could require additional organic functionalization to increase their solubility in non-aqueous media, if further studies of the type reported here are to be pursued. Additionally, binding sites for uranyl that offer more than four donor atoms could preclude the need for solvent coordination in the equatorial "belt" of the uranyl ion and thus could aid in stabilizing reduced forms of these compounds. Nevertheless, the successful measurement of the electrochemical properties of the

heterobimetallic uranyl compounds containing redox-active metals reported here do encourage further exploration into the development of synthetic strategies for preparation of compounds of this type and, in turn, elucidation of their diverse properties.

Conclusion

We have prepared and characterized a family of metalloligands based upon the Group 10 metals Ni, Pd, and Pt. Observations surrounding the reactivity of these metalloligands with uranyl reveal that heterobimetallic complexes of Ni(II), Pd(II), and Pt(II) with uranyl are accessible, although difficulties with solubility, purification, and stability were encountered moving down the group. Structural data revealed the square-planar environments for the Group 10 metals in all cases, with uranyl situated in a tetradentate site in the case of **[Ni,UO_2]**. Investigations of the electrochemical properties of the bimetallic complexes of **[Ni,UO_2]** and **[Pd,UO_2]** demonstrate that multiple redox events are accessible in the systems, findings that could encourage further studies into complexes of this type. However, the modest solubilities of the bimetallic species in most solvents suggest that pursuit of improved solubility could be enabling for future studies of bimetallic complexes of the type described in this report.

Experimental Section

General Considerations

All manipulations were carried out in dry N_2-filled gloveboxes (Vacuum Atmospheres Co., Hawthorne, CA) or under N_2 atmosphere using standard Schlenk techniques unless otherwise noted. All solvents were of commercial grade and dried over activated alumina using a PPT Glass Contour (Nashua, NH) solvent purification system prior to use, and were stored over molecular

sieves. $\mathbf{L^{OH}}$ and **[Ni]** were prepared according to literature procedure, as were $\mathbf{L^{OMe}}$ and uranyl triflate.[12,15,34] Deuterated solvents were purchased from Cambridge Isotope Laboratories. ^{1}H and ^{13}C NMR spectra were collected on 400 or 500 MHz Bruker spectrometers (Bruker, Billerica, MA, USA) and referenced to the residual protio-solvent signal.[35] Infrared spectra were collected on the benchtop in open atmosphere using a Shimadzu IRSpirit Fourier Transform infrared spectrometer in transmission mode using KBr solid pellets. Elemental analysis of **[Pd]** was performed at the University of Memphis (Memphis, TN, USA), analysis of **[Pt]** was performed by Midwest Microlab, Inc. (Indianapolis, IN, USA), and analysis of **[Ni,UO_2]** was performed at the CENTC Elemental Analysis Facility at the University of Rochester.

X-ray Crystallography

Crystals were mounted using Paratone oil with MiTeGen loops and placed under a cold nitrogen stream for data collection. Low temperature (100 K) X-ray data for **[Pd]**, **[Pt]**, and **[Ni,UO_2]** were collected using 1°-wide ω- or φ-scans on a Bruker D8 Venture diffractometer with a Photon III CPAD detector equipped with Helios high-brilliance multilayer mirror optics. X-rays were provided by a IμS 3.0 Microfocus Mo sealed tube running at 50 kV and 1.4 mA (Mo Kα = 0.71073 Å). All data manipulations were carried out using the Bruker APEX4 Software Suite.[36,37] The data sets for **[Pd]** and **[Pt]** were corrected for absorption using the multi-scan method by SADABS, while a numerical face-indexed absorption correction was used for **[Ni,UO_2]**.[38] SHELXT was used to solve each structure using intrinsic phasing methods.[39] Final stages of weighted full-matrix least-squares refinement were conducted using F_o^2 data with SHELXL in SHELXle and/or in the Olex2 software package.[40,41,42]

All non-hydrogen atoms were refined anisotropically. Non-methyl hydrogen atoms bonded to carbon in each complex were fixed at idealized riding model sp^2- or sp^3-hybridized positions with

C–H bond lengths of 0.95 - 0.99 Å. Methyl groups were incorporated into the structural models either as sp^3-hybridized riding model groups with idealized "staggered" geometry and a C–H bond length of 0.98 Å or as idealized riding model rigid rotors (with a C–H bond length of 0.98 Å) that were allowed to rotate freely about their C–C or O–C bonds in least-squares refinement cycles. The isotropic thermal parameters of the idealized hydrogen atoms in all structures were fixed at values 1.2 (non-methyl) or 1.5 (methyl) times the equivalent isotropic thermal parameter of the carbon atom to which they are covalently bonded. The relevant crystallographic and structure refinement data for the structures are given in Table S3.

Electrochemistry

Electrochemical experiments were carried out in a nitrogen-filled glove box. Tetra(n-butylammonium) hexafluorophosphate (Sigma-Aldrich, electrochemical grade; 0.1 M in the indicated solvent) served as the supporting electrolyte for all experiments. Measurements were made with a Gamry Reference 600 Plus Potentiostat/Galvanostat using a standard three-electrode configuration. The working electrode was the basal plane of highly oriented pyrolytic graphite (HOPG) (GraphiteStore.com, Buffalo Grove, IL; surface area: 0.09 cm2), the counter electrode was a platinum wire (Kurt J. Lesker, Jefferson Hills, PA; 99.99%, 0.5 mm diameter), and a silver wire immersed in electrolyte served as a pseudo-reference electrode (CH Instruments). The reference was separated from the working solution by a Vycor frit (Bioanalytical Systems, Inc.). For all uranium complexes, a platinum wire directly immersed in the working solution was used as a quasi-reference electrode. Ferrocene (Sigma Aldrich, twice-sublimed; 0.1 M) was added to the electrolyte solution at the conclusion of each experiment and the midpoint potential of the ferrocenium/ferrocene couple (denoted as $Fc^{+/0}$) served as an external standard for comparison of the recorded potentials.

Synthetic Procedures

Synthesis of **[Pd]**. To a solution of $\mathbf{L^{OH}}$ (0.06 g, 0.18 mmol) in methanol (5 mL) was added $[Pd(OAc)_2]_3$ (0.036 g, 0.16 mmol) in methanol (20 mL) as a suspension. The solution immediately changed from yellow in color to red and was allowed to stir at room temperature in open air. After stirring for 12 hrs, the yellow solution was concentrated and the resulting powder stirred in diethyl ether to yield a yellow-green solid. This was isolated by filtration and washed with diethyl ether to yield **[Pd]** (0.064 g, 93%). ^{1}H NMR (500 MHz, CD_3CN) δ (ppm): 7.94 (s, 1H), 7.89 (s, 1H), 7.19 (d, 2H, J = 6.9 Hz), 6.94 (d, 1H, J = 6.6 Hz), 6.87 (t, 3H, J = 8.3 Hz), 6.52 (q, 2H, J = 7.5 Hz), 3.72 (s, 2H), 1.55 (s, 6H). ^{13}C{^{1}H} NMR (126 MHz, CD_3CN) δ (ppm): 59.80, 56.72, 52.76, 52.20, 47.48, 47.35, 24.07, 23.50, 19.17, 18.99, 14.44, 14.39. IR spectroscopy (KBr): ν (cm^{-1}) = 1638 (s, C=N stretching), 1547 (m, C=C stretching), 1300 (s, aromatic ether C–O stretching), 729 (m, 1,2,3-substituted ring sp^2 C–H bending). Anal. Calcd for $C_{18}H_{18}N_2O_4Pd$ (**[Pd]**): C 49.96, H 4.19, N 6.47; Found: C 49.35, H 4.65, N 6.75. Calc for $C_{18}H_{18}N_2O_4Pd$ + 0.25 H_2O: C 49.44, H 4.26, N 6.41. This analysis is consistent with the incorporation of 0.25 equiv. of water during sample handling. Single crystals suitable for X-ray diffraction were grown by vapor diffusion of pentane into a concentrated solution of **[Pd]** in tetrahydrofuran.

Synthesis of **[Pt]**. To a solution of $\mathbf{L^{OMe}}$ (0.39 g, 1.1 mmol) in DMF (40 mL) was added sodium acetate (0.18 g, 2.2 mmol). The solution was allowed to stir for 10 minutes at 95 ºC, after which $PtCl_2(DMSO)_2$ (0.37 g, 1.1 mmol) in DMSO (5 mL) was added dropwise to the solution. This mixture was then stirred at 95 ºC for an additional 5 hrs before it was cooled to room temperature and the product precipitated by the addition of water (150 mL). After storage at 4 ºC for several hours, the precipitate was isolated via filtration as a yellow solid and washed with diethyl ether to yield **[Pt]** (0.44 g, 72%). ^{1}H NMR (500 MHz, CD_3CN) δ (ppm): 8.28 (s, 1H), 8.23 (s, 1H), 7.11

(dd, J = 8.2 Hz, 1H), 7.03 (td, J = 7.2, 2.0 Hz, 3H), 6.62 – 6.54 (m, 2H), 3.84 (s, 6H), 3.70 (d, J = 1.3 Hz, 2H), 1.57 (s, 6H). IR spectroscopy (KBr): ν (cm^{-1}) = 1629 (m, C=N stretching), 1546 (w, C=C stretching), 1314 (s, aromatic ether C–O stretching), 734 (m, 1,2,3-substituted ring sp^2 C–H bending). Anal. Calcd for $C_{20}H_{22}N_2O_4Pt$ (**[Pt]**): C 43.72, H 4.04, N 5.10; Found C 44.47, H 4.30, N 5.27. Calc for $C_{20}H_{22}N_2O_4Pt$ + 0.25 CH_3CN: C 43.99, H 4.1, N 5.63. This analysis is consistent with the incorporation of 0.25 equiv. of acetonitrile during sample handling. Single crystals suitable for X-ray diffraction were grown by vapor diffusion of diethyl ether into a concentrated solution of **[Pt]** in acetonitrile.

Synthesis of **[Ni,UO_2]**. To a suspension of **[Ni]** (0.10 g, 0.26 mmol) in acetonitrile (100 mL) was added uranyl acetate dihydrate (0.10 g, 0.24 mmol) in acetonitrile (50 mL) and the resulting mixture was stirred under refluxing conditions for 4 hrs. Following reflux, a brown powder was isolated by filtration and washed with diethyl ether to yield **[Ni,UO_2]** as a red-brown solid (0.120 g, 73%). ^{1}H NMR (500 MHz, d_6-DMSO) δ (ppm): 8.10 (d, 2H, J = 3.7 Hz), 6.78 (m, 3H), 6.69 (m, 1H), 6.54 (m, 2H), 3.65 (s, 2H), 1.59 (s, 6H). ^{13}C{^{1}H} NMR (126 MHz, d_6-DMSO) δ (ppm): 163.83, 161.76, 161.61, 161.18, 153.64, 153.11, 120.11, 120.00, 118.86, 118.84, 118.63, 118.53, 118.40, 118.01, 70.05, 68.06, 25.49. IR spectroscopy (KBr): ν (cm^{-1}) = 1605 (s, C=N stretching), 1542 (s, C=C stretching), 1260 (s, aromatic ether C–O stretching), 918 (s, $[UO_2]_{asymm}$), 732 (m, 1,2,3-substituted ring sp^2 C–H bending). Anal. Calcd for $C_{18}H_{16}N_2O_6NiU$ (**[Ni,UO_2]**): C 33.11, H 2.47, N 4.29; Found: C 31.49, H 2.41, N 3.96. Calc for $C_{18}H_{18}N_2O_7NiU$ + 0.4 H_2O: C 31.87, H 2.79, N 4.13. This analysis is consistent with the incorporation of 0.4 equiv. of water during sample handling. Single crystals suitable for X-ray diffraction were grown by vapor diffusion of diethyl ether into a concentrated solution of **[Ni, UO_2]** in dimethylformamide.

Synthesis of **[Pd,UO_2]**. To a suspension of **[Pd]** (0.05 g, 0.11 mmol) in acetonitrile (30 mL) was added uranyl acetate dihydrate (0.05 g, 0.11 mmol) in acetonitrile (20 mL) and the resulting mixture was stirred under refluxing conditions for 4 hrs. Following reflux, a brown powder was isolated by filtration and washed with diethyl ether and acetonitrile to yield **[Pd,UO_2]** as a red-brown solid (0.06 g, ~50%). The isolated solids obtained from multiple attempts at synthesis of **[Pd,UO_2]** contained ~15% impurities in each case of unreacted **[Pd]** that could not be separated from the component of the product mixture that appeared to be the desired product. ^{1}H NMR (500 MHz, *d*$_6$-DMSO) δ (ppm): 8.42 (s, 1H), 8.36 (s, 1H), 6.82 (m, 3H, J = 7.2 Hz), 6.76 (m, 1H), 6.67 (m, 2H), 4.10 (s, 2H), 1.64 (s, 6H). IR spectroscopy (KBr): ν (cm^{-1}) = 1656 (m, C=N stretching), 1500 (w, C=C stretching), 1266 (m, aromatic ether C–O stretching), 912 (s, $[UO_2]_{asymm}$), 732 (m, 1,2,3-substituted ring sp^2 C–H bending).

Associated Content

Supporting Information. The following files are available free of charge:

NMR spectra, characterization data for the complexes reported here, and detailed information regarding the single-crystal X-ray diffraction analysis (PDF)

Cartesian coordinates for the structures from XRD (CIF, XYZ)

Author Information

Corresponding Authors

James D. Blakemore − Department of Chemistry, University of Kansas, Lawrence, Kansas 66045, United States; orcid.org/0000-0003-4172-7460; Phone: +1 (785) 864-3019; E-mail: blakemore@ku.edu

Authors

Emily R. Mikeska - Department of Chemistry, University of Kansas, Lawrence, Kansas 66045, United States; orcid.org/0000-0001-5149-0132

Natalie M. Lind - Department of Chemistry, University of Kansas, Lawrence, Kansas 66045, United States

Alexander C. Ervin - Department of Chemistry, University of Kansas, Lawrence, Kansas 66045, United States

Celine Khalife - Department of Chemistry, University of Kansas, Lawrence, Kansas 66045, United States

Joseph P. Karnes - Department of Chemistry, University of Kansas, Lawrence, Kansas 66045, United States

Author Contributions

The manuscript was written through contributions of E.R.M. and J.D.B. All the authors contributed to the design and/or execution of the experimental work reported here. All authors have given approval to the final version of the manuscript.

Acknowledgement

The authors thank Dr. William Brennessel (CENTC Elemental Analysis Facility, University of Rochester funded by NSF CHE-0650456) for assistance with elemental analysis. This work was supported by the U.S. Department of Energy, Office of Science, Office of Basic Energy Sciences through the Early Career Research Program (DE-SC0019169). N.M.L. was supported by NSF REU Program in Chemistry at the University of Kansas (CHE-1950293), and E.R.M., A.C.E., and

J.P.K. were supported by a U.S. National Science Foundation Research Traineeship (NRT) at the University of Kansas (DGE-1922649).

References

[1] Costa Peluzo, B. M. T.; Kraka, E. Uranium: The Nuclear Fuel Cycle and Beyond. *Int. J. Mol. Sci.*, **2022**, *23*, 4655.

[2] (a) Morgensern, A.; Apostolidis, C.; Carlos-Marquez, R.; Mayer, K.; Molinet, R. Single-column extraction chromatographic separation of U, Pu, Np and Am. *Radiochim. Acta.*, **2002**, *90*, 81–85. (b) Graser, C.-H.; lal Banik, N.; Bender, K. A.; Lagos, M.; Marquardt, C. M.; Marsac, R.; Montoya, V.; Geckis, H. Sensitive Redox Speciation of Iron, Neptunium, and Plutonium by Capillary Electrophoresis Hyphenated to Inductively Coupled Plasma Sector Field Mass Spectrometry. *Anal. Chem.*, **2015**, *87*, 9786–9794. (c) McCan, K.; Sinkov, S. I.; Lumetta, G. J.; Shafer, J. C. Organic and Aqueous Redox Speciation of Cu(III) Periodate Oxidized Transuranium Actinides. *Ind. Eng. Chem. Res.*, **2018**, *57*, 1277–1283. (d) Agarwal, R.; Sharma, M. K. Selective Electrochemical Separation and Recovery of Uranium from Mixture of Uranium(VI) and Lanthanide(III) Ions in Aqueous Medium. *Inorg. Chem.*, **2018**, *57*, 10984–10992. (e) Kumar, S. S.; Srivastava, A.; Rao, A.; Chatterjee, S.; Gamre, S. Selective separation of neptunium on microporous bifunctional anion exchange resin aided by redox speciation. *Hydrometallurgy*, **2021**, *203*, 105642.

[3] Sadergaski, L. R.; Stoxen, W.; Hixon, A. E. Uranyl Peroxide Nanocluster (U_{60}) Persistence and Sorption in the Presence of Hematite. *Environ. Sci. Technol.*, **2018**, *52*, 3304–3311. (b) Hua, Y.; Wang, W.; Hu, N.; Gu, T.; Ling, L.; Zhang, W. Enrichment of uranium from wastewater with nanoscale zero-valent iron (nZVI). *Environ. Sci.: Nano.*, **2021**, *8*, 666–674. (c) You, W.; Peng, W.; Tian, Z.; Zheng, M. Uranium bioremediation with U(VI)-reducing bacteria. *Sci. Total Environ.*, **2021**, *798*, 149107.

[4] Neidig, M. L.; Clark, D. L.; Martin, R. L. Covalency in *f*-element complexes. *Coord. Chem. Rev.*, **2013**, *257*, 394–406.

[5] (a) Saha, B.; Venatesan, K. A.; Ntarajan, R.; Antony, M. P.; Rao, P. R. V. Studies on the extraction of uranium by N-octanoyl-N-phenylhydrozamic acid. *Radiochim. Acta*, **2002**, *90*, 455–459. (b) Beer, P. D.; Brindley, G. D.; Fox, O. D.; Grieve, A.; Ogden, M. I.; Szemes, F.; Drew, M. G. B. Acid-amide calixarene ligands for uranyl and lanthanide ions: synthesis, structure coordination and extraction studies. *J. Chem. Soc., Dalton Trans.*, **2002**, 3101. (c) Bharara, M. S.; Strawbridge, K.; Vilsef, J. Z.; Bray, T. H.; Gorden, A. E. V. Novel Dinuclear Uranyl Complexes with Asymmetric Schiff Base Ligands: Synthesis, Structural Characterization, Reactivity, and Extraction Studies. *Inorg. Chem.*, **2007**, *46*, 8309–8315.

[6] (a) Sarsfield, M. J.; Helliwell, M. Extending the Chemistry of the Uranyl Ion: Lewis Acid Coordination to a U=O Oxygen. *J. Am. Chem. Soc.*, **2004**, *126*, 1036–1037. (b) Hayton, T. W.; Wu, G. Exploring the Effects of Reduction or Lewis Acid Coordination on the U=O Bond of the Uranyl Moiety. *Inorg. Chem.*, **2009**, *48*, 3065–3072. (c) Bell, N. L.; Shaw, B.; Arnold, P. L.; Love, J. B. Uranyl to Uranium(IV) Conversion through Manipulation of Axial and Equatorial Ligands. *J. Am. Chem. Soc.*, **2018**, *140*, 3378–3384.

[7] (a) Arnold, P. L.; Patel, D.; Wilson, C.; Love, J. B. Reduction and selective oxo group silylation of the uranyl dication. *Nature*, **2008**, *451*, 315–317. (b) Schnaars, D. D.; Qu, G.; Hayton, T. W. Reduction of Pentavalent Uranyl to U(IV) Facilitated by Oxo Functionalization. *J. Am. Chem. Soc.*, **2009**, *131*, 17532–17533. (c) Schnaars, D. D.; Wu, G.; Hayton, T. W. Borane-Mediated Silylation of a Metal-Oxo Ligand. *Inorg. Chem.*, **2011**, *50*, 4695–4697. (d) Cowie,

B. E.; Nichol, G. S.; Love, J. B.; Arnold, P. L. Double uranium oxo cations derived from uranyl by borane or silane reduction. *Chem. Commun.*, **2018**, *54*, 3839–3842.

[8] (a) Arnold, P. L.; Love, J. B.; Patel, D. Pentavalent uranyl complexes. *Coord. Chem. Rev.*, **2009**, *253*, 1973 – 1978. (b) Fortier, S.; Hayton, T. W. Oxo ligand functionalization in the uranyl ion (UO_2^{2+}). *Coord. Chem. Rev.*, **2010**, *254*, 197–214. (c) Cowie, B. E.; Purkis, J. M.; Austin, J.; Love, J. B.; Arnold, P. L. Thermal and Photochemical Reduction and Functionalization Chemistry of the Uranyl Dication, $[U^{VI}O_2]^{2+}$. *Chem. Rev.*, **2019**, *119*, 10595–10637.

[9] (a) Nocton, G.; Horeglad, P.; Vetere, V.; Pécaut, J.; Dubois, L.; Maldivi, P.; Edelstein, N. M.; Mazzanti, M. Synthesis, Structure, and Bonding of Stable Complexes of Pentavalent Uranyl. *J. Am. Chem. Soc.*, **2010**, *132*, 495–508. (b) Pankhurst, J. R.; Bell, N. L.; Zegke, M.; Platts, L. N.; Lamfsus, C. A.; Maron, L.; Natrajan, L. S.; Sproules, S.; Arnold, P. L.; Love, J. B. Inner-sphere vs. outer-sphere reduction of uranyl supported by a redox-active, donor-expanded dipyrrin. *Chem. Sci.*, **2017**, *8*, 108–116. (c) Ghosh, T. K.; Mahapatra, P.; Drew, M. G. B.; Franconetti, A.; Frontera, A.; Ghosh, A. The Effect of Guest Metal Ions on the Reduction Potentials of Uranyl(VI) Complexes: Experimental and Theoretical Investigations. *Chem. – Eur. J.*, **2019**, *26*, 1612–1623. (d) Ghosh, T. K.; Maity, S.; Ghosh, S.; Gomila, R. M.; Frontera, A.; Ghosh, A. Role of Redox-Inactive Metal Ions in Modulating the Reduction Potential of Uranyl Schiff Base Complexes: Detailed Experimental and Theoretical Studies. *Inorg. Chem.*, **2022**, *61*, 7130–7142.

[10] Kumar, A.; Lionetti, D.; Day, V. W.; Blakemore, J. D. Redox-Inactive Metal Cations Modulate the Reduction Potential of the Uranyl Ion in Macrocyclic Complexes. *J. Am. Chem. Soc.*, **2020**, *142*, 3032–3041.

[11] Dopp, C. M.; Golwankar, R. R.; Kelsey, S. R.; Douglas, J. T.; Erickson, A. N.; Oliver, A. G.; Day, C. S.; Day, V. W.; Blakemore, J. D. Vanadyl as a Spectroscopic Probe of Tunable Ligand Donor Strength in Bimetallic Complexes. *Inorg. Chem.*, **2023**, *62*, 9827–9843.

[12] Casellato, U.; Guerriero, P.; Tamburini, S.; Vigato, P. A. Mononuclear, homo- and heteropolynuclear complexes with acyclic compartmental Schiff bases. *Inorg. Chim. Acta.*, **1993**, *207*, 39–58.

[13] Salmon, L.; Thuéry, P.; Ephritikhine, M. Crystal structure of hetero(bi- and tetra-)metallic complexes of compartmental Schiff bases uniting uranyl and transition metal (Ni^{2+}, Cu^{2+}) ions. *Polyhedron*, **2003**, *22*, 2683–2688.

[14] Faizova, R.; White, S.; Scopelliti, R.; Mazzanti, M. The effect of iron binding on uranyl(V) stability. *Chem. Sci.*, **2018**, *9*, 7520–7527.

[15] Berthet, J. C.; Lance, M.; Nierlich, M.; Ephritikhine, M. Simple Preparations of the Anhydrous and Solvent-Free Uranyl and Cerium(IV) Triflates $UO_2(OTf)_2$ and $Ce(OTf)_4$ – Crystal structures of $UO_2(OTf)_2(py)_3$ and $[\{UO_2(py)_4\}_2(\mu\text{-}O)][OTf]_2$. *Eur. J. Inorg. Chem.*, **2000**, *9*, 1969–1973.

[16] Hobday, M. D.; Smith, T. D. N,N'-Ethylenebis(salicylideneiminato) Transition Metal Ion Chelates. *Coord. Chem. Rev.*, **1973**, *9*, 311–337.

[17] Calligaris, M.; Nardin, G.; Randaccio, L. Structural aspects of metal complexes with some tetradentate Schiff bases. *Coord. Chem. Rev.*, **1972**, *7*, 385–403.

[18] Golwankar, R. R.; Kumar, A. Day, V. W.; Blakemore, J. D. Revealing the Influence of Diverse Secondary Metal Cations on Redox-Active Palladium Complexes. *Chem. Eur. J.*, **2022**, *28*, e202200344.

[19] Song, Y.; Yang, Y.; Medforth, C. J.; Pereira, E.; Singh, A. K.; Xu, H.; Jiang, Y.; Brinker, C. J.; van Swol, F.; Shelnutt, J. A. Controlled Synthesis of 2-D and 3-D Dendritic Platinum Nanostructures. *J. Am. Chem. Soc.*, **2004**, *126*, 635–645.

[20] Wang, L.; Imura, M.; Yamauchi, Y. Tailored Design of Architecturally Controlled Pt Nanoparticles with Huge Surface Areas towards Superior Unsupported Pt Electrocatalysts. *ACS Appl. Mater. Interfaces*, **2021**, *4*, 2865–2869.

[21] Liu, Y.; Wu, H.; Chong, Y.; Wamer, W. G.; Xia, Q.; Cia, L.; Nie, Z.; Fu, P. P.; Yin, J.-J. Platinum Nanoparticles: Efficient and Stable Catechol Oxidase Mimetics. *ACS Appl. Mater. Interfaces*, **2015**, *7*, 19709–19717.

[22] (a) Shimazaki, Y.; Yajima, T.; Tani, F.; Karasawa, S.; Fukui, K.; Naruta, Y.; Yamauchi, O. Syntheses and Electronic Structures of One-Electron-Oxidized Group 10 Metal(II)-(Disalicylidene)diamine Complexes (Metal = Ni, Pd, Pt). *J. Am. Chem. Soc.*, **2007**, *129*, 2559–2568. (b) Kurahashi, T.; Fujii, H. One-Electron Oxidation of Electronically Diverse Manganeses(III) and Nickel(II) Salen Complexes: Transition from Localized to Delocalized Mixed-Valent Ligand Radicals. *J. Am. Chem. Soc.*, **2011**, *133*, 8307–8316. (c) Lyons, C. T.; Stack, T. D. P. Recent advances in phenoxyl radical complexes of salen-type ligands as mixed-valent galactose oxidase models. *Coord. Chem. Rev.*, **2013**, *257*, 528–540.

[23] Mikeska, E. R.; Ervin, A. C.; Zhang, K.; Benitez, G. M.; Powell, S. M. R.; Oliver, A. G.; Day, V. W.; Caricato, M.; Comadoll, C. G.; Blakemore, J. D. Evidence for Uranium(VI/V) Redox Supported by 2,2′-Bipyridyl-6,6′-2 dicarboxylate. *Inorg. Chem.*, **2023**, *in press*, doi: 10.1021/acs.inorgchem.3c02397

[24] The case of **[Pt]** necessitated a different uranyl-containing metalation reagent, as installation of UO_2^{2+} in the tetradentate site provided by **[Pt]** is unlikely to be facilitated by a precursor containing counteranions that can undergo protonolysis. An attempt at synthesis of **[Pt,UO$_2$]** by addition of 1 equiv. of $UO_2(OTf)_2$ to **[Pt]** in d_3-MeCN was carried out; the ^{1}H NMR of the reaction mixture (see SI, Figure S23) is suggestive of formation of a heterobimetallic adduct. However, further purification and isolation of the desired product were impeded by the apparent instability of the adduct; removal of d_3-MeCN *in vacuo* followed by exposure of the resulting solid to tetrahydrofuran resulted in a marked color change and decomposition.

[25] Yang, L.; Powell, D. R.; Houser, R. P. Structural variation in copper(I) complexes with pyridylmethylamide ligands: structural analysis with a new four-coordinate geometry index, τ_4. *Dalton Trans.*, **2007**, 955–964.

[26] Shannon, R. D. Revised Effective Ionic Radii and Systematic Studies of Interatomic Distances in Halides and Chalcogenides. *Acta Cryst.*, **1976**, *A32*, 751–767.

[27] Jeffery, G. A. *An Introduction to Hydrogen Bonding.*, Oxford University Press: New York, NY, **1997**, p. 12.

[28] Desiraju, G. R. The C–H•••O Hydrogen Bond in Crystals: What Is It? *Acc. Chem. Res.*, **1991**, *24*, 290–296.

[29] Cowie, B. E.; Purkis, J. M.; Austin, J.; Love, J. B.; Arnold, P. L. Thermal and Photochemical Reduction and Functionalization Chemistry of the Uranyl Dication $[U^{VI}O_2]^{2+}$. *Chem. Rev.*, **2019**, *119*, 10595–10637.

[30] Isse, A. A.; Gennaro, A.; Vianello E. A study of the electrochemical reduction mechanism of Ni(salophen) in DMF. *Electrochim. Acta*, **1992**, *37*, 113–118.

[31] Mikeska, E. R.; Blakemore, J. D. Evidence for Reactivity of Decamethylcobaltocene with Dichloromethane. *Organometallics*, **2023**, *42*, 1444–1447.

[32] Golwankar, R. R.; Makoz, M. Z.; Cajiao, N.; Neidig, M. L.; Oliver, A. G.; Day, C. S.; Day, V. W.; Glezakou, V.-A., Blakemore, J. D. Electrochemical Activation and Functionalization of the Uranyl Ion. *ChemRxiv*, **2023**, doi: 10.26434/chemrxiv-2023-gnbpd.

[33] Golwankar, R. R.; Curry, T. D., II; Paranjothi, C. J.; Blakemore, J. D. Molecular Influences on the Quantification of Lewis Acidity with Phosphine Oxide Probes. *Inorg. Chem.* **2023,** *62*, 9765-9780.

[34] Bermejo, M. R.; Fernández, M. I.; Gómez-Fórneas, E.; González-Noya, A.; Maneiro, M.; Pedrido, R.; Rodríguez, M. J. Self-Assembly of Dimeric Mn^{III}–Schiff-Base Complexes Tuned by Perchlorate Anions. *Eur. J. Inorg. Chem.*, **2007**, 3789–3797.

[35] Fulmer, G. R.; Miller, A. J.; Sherden, N. H.; Gottlieb, H. E.; Nudelman, A.; Stoltz, B. M.; Bervaw, E.; Goldberg, K. I. NMR Chemical Shifts of Trace Impurities: Common Laboratory Solvents, Organics, and Gases in Deuterated Solvents Relevant to the Organometallic Chemist. *Organometallics*, **2010**, *29*, 2176–2179.

[36] *APEX-4.* Bruker Analytical X-ray Systems Inc.: Madison, WI, USA, 2022.

[37] *SAINT Ver. 8.40A*. Bruker Analytical X-ray Systems Inc.: Madison, WI, USA, 2022.

[38] Krause, L.; Herbst-Irmer, R; Sheldrick, G. M.; Stalke, D. Comparison of Silver and Molybdenum Microfocus X-ray Sources for Single-Crystal Structure Determination. *J. Appl. Cryst*, **2015**, *48*, 3.

[39] Sheldrick, G. M. SHELXT – Integrated Space-Group and Crystal-structure Determination. *Acta Crystallogr., Sect. A: Found. Crystallogr.*, **2015**, *A71*, 3–8.

[40] Sheldrick, G. M. Crystal structure refinement with SHELXL. *Acta Crystallogr., Sect. C: Struct. Chem.* **2015,** *71*, 3-8.

[41] Hübschle, C. B.; Sheldrick, G. M; Dittrich, B. ShelXle: a Qt Graphical User Interface for SHELXL. *J. Appl. Cryst.*, **2011**, *44*, 1281–1284.

[42] Dolomanov, O. V.; Bourhis, L. J.; Gildea, R. J.; Howard, J. A. K.; Puschmann, H., OLEX2: a complete structure solution, refinement and analysis program. *J. Appl. Crystallogr.* **2009,** *42*, 339–341.